LHC discovery potential of the lightest NMSSM Higgs boson in the $h_1 \to a_1 a_1 \to 4\mu$ channel

Alexander Belyaev,[1,2] Jim Pivarski,[3] Alexei Safonov,[3] Sergey Senkin,[3] and Aysen Tatarinov[3]

[1]*School of Physics & Astronomy, University of Southampton, Highfield, Southampton SO17 1BJ, United Kingdom*
[2]*Particle Physics Department, Rutherford Appleton Laboratory, Chilton, Didcot, Oxon OX11 0QX, United Kingdom*
[3]*Department of Physics and Astronomy, Texas A&M University, College Station, Texas 77843, USA*

(Received 3 March 2010; published 26 April 2010)

We explore the potential of the Large Hadron Collider to observe the $h_1 \to a_1 a_1 \to 4\mu$ signal from the lightest scalar Higgs boson (h_1) decaying into the two lightest pseudoscalar Higgs bosons (a_1), followed by their decays into four muons in the next-to-minimal supersymmetric standard model (NMSSM). The signature under study applies to the region of the NMSSM parameter space in which $m_{a_1} < 2m_\tau$, which has not been studied previously. In such a scenario, the suggested strategy of searching for a four-muon signal with the appropriate background suppression would provide a powerful method to discover the lightest *CP*-even and *CP*-odd NMSSM Higgs bosons h_1 and a_1.

DOI: 10.1103/PhysRevD.81.075021 PACS numbers: 14.80.Da, 12.60.Jv

I. INTRODUCTION

The next-to-minimal supersymmetric standard model (NMSSM) [1–13] extends the particle content of the minimal supersymmetric standard model (MSSM) by one singlet superfield. The NMSSM has several attractive features beyond the MSSM. First, the NMSSM elegantly solves the so-called μ problem [14]: the scale of the μ parameter is dynamically generated at the electroweak or supersymmetry (SUSY) scale when the singlet Higgs acquires a vacuum expectation value (VEV). Second, the fine-tuning and little hierarchy problems of the NMSSM are greatly diminished compared to the MSSM [15]. In the NMSSM, the upper mass limit on the lightest *CP*-even Higgs boson is higher than in the MSSM, making it less constrained experimentally. Another attractive feature of the NMSSM is that the lightest *CP*-even Higgs can have a significant branching fraction for the new $h_1 \to a_1 a_1$ decay (h_1 and a_1 are the lightest *CP*-even and *CP*-odd Higgs bosons, respectively). This weakens the LEP-II constraints on the allowed Higgs parameter space, as this new decay channel reduces the branching fractions of h_1 into the modes used in direct Higgs searches. In addition, there are interesting implications in the cosmological dark matter sector of the model due to the appearance of the fifth neutralino, the ''singlino.'' It has been shown [16] that the NMSSM is consistent with the experimentally measured relic density, and the data provide important constraints on the allowed NMSSM parameters.

The rich phenomenology offered by the NMSSM, stemming from the extension of the scalar sector, has been the focus of numerous studies [17–25]. In Ref. [18], the first attempt to establish a ''no-lose'' theorem for NMSSM was presented. This theorem states that the Large Hadron Collider (LHC) has the potential to discover at least one NMSSM Higgs boson in the conventional mode, assuming that Higgs-to-Higgs decay modes are not important. However, the fact that Higgs-to-Higgs decay modes can be important has been shown in analyses devoted to reestablishing the no-lose theorem [19–25] in the case where the $h_1 \to a_1 a_1$ branching fractions are significant and a_1 is light. NMSSM scenarios with m_{a_1} between the 2τ and $2b$-quark thresholds ($2m_\tau < m_{a_1} < 2m_b$) have previously been considered, focusing on the 4τ [25] channels in Higgs-strahlung and vector boson fusion, establishing the NMSSM no-lose theorem at the LHC [25] for this a_1 mass region. Future analysis of the 4τ channel is likely to be technically challenging and can only be performed with large data sets (typical integrated luminosity of 10–100 fb^{-1}). A more recent study [26] has focused on the same region using the $h_1 \to a_1 a_1 \to 2\mu 2\tau$ process, which has the benefit that the invariant mass of two muons forms a much narrower peak, improving the sensitivity of such an analysis in spite of the large reduction in signal yield due to small $\mathcal{B}(a_1 \to \mu\mu)$. Our findings indicate a substantially higher QCD multijet background contamination as compared to Ref. [26], which may have a substantial effect of the sensitivity of such a search.

In this paper, we explore the region in which the a_1 mass is below the 2τ threshold ($m_{a_1} < 2m_\tau$). For this case, which has not been studied previously, we explore the potential of the $h_1 \to a_1 a_1 \to 4\mu$ signature at the LHC. Unlike searches for the 4τ signature, the invariant mass of each muon pair provides a direct estimate of m_{a_1} and the 4μ invariant mass provides m_{h_1}. The use of these kinematic constraints leads to essentially zero background and therefore allows one to rely on direct gg and $b\bar{b}$ fusion for Higgs production instead of the subdominant vector boson fusion or associated production processes chosen in the 4τ search [18] to suppress QCD backgrounds.

We demonstrate that the analysis of the 4μ mode has excellent sensitivity to h_1 production, can be performed with early LHC data, and requires little in terms of detector performance except reasonably robust muon tracking and identification. To present a realistic analysis, we use parameters of the Compact Muon Solenoid (CMS) detector at

the LHC to design event selection and to estimate background contributions.

The rest of the paper is organized as follows. In Sec. II, we study the NMSSM parameter space in which $m_{a_1} < 2m_\tau$ and discuss the phenomenology of the model. In Sec. III, we review constraints on the NMSSM parameter space from existing data. In Sec. IV, we outline the proposed analysis for the 4μ mode and evaluate its sensitivity. Final conclusions are presented in Sec. V.

II. NMSSM PARAMETER SPACE

In our study we consider the simplest version of the NMSSM [1–12], in which the $\mu\hat{H}_1\hat{H}_2$ term of the MSSM superpotential is replaced by

$$\lambda\hat{S}\hat{H}_1\hat{H}_2 + \frac{\kappa}{3}\hat{S}^3, \tag{1}$$

making the superpotential scale invariant. In general, there are five soft breaking terms; in the ''nonuniversal'' case,

$$m_{H_1}^2 H_1^2 + m_{H_2}^2 H_2^2 + m_S^2 S^2 + \lambda A_\lambda H_1 H_2 S + \frac{\kappa}{3} A_\kappa S^3. \tag{2}$$

In the above equations, capital letters with tildes denote superfields, while symbols without tildes denote the scalar component of the respective superfield.

Soft breaking parameters in Eq. (2), $m_{H_1}^2$, $m_{H_2}^2$, and m_S^2, can be expressed in terms of M_Z, the ratio of the doublet Higgs VEVs, $\tan\beta$, and $\mu = \lambda s$ (where $s = \langle S \rangle$, the VEV of the singlet Higgs field) through the three minimization equations of the Higgs potential. Assuming that the Higgs sector is CP-conserving, the NMSSM Higgs sector at the electroweak scale is uniquely defined by 14 parameters: $\tan\beta$, the trilinear couplings in the superpotential, λ and κ, the corresponding soft SUSY breaking parameters A_λ and A_κ, the effective μ parameter $\mu = \lambda s$, the gaugino mass parameters M_1, M_2, and M_3, the squark and slepton trilinear couplings A_t, A_b, and A_τ, and the squark and slepton mass parameters M_{f_L} and M_{f_R}. For simplicity, we assume universality within three generations for the last two parameters, leaving only six parameters for sfermion masses.

A. Parameter scan of the low-m_{a_1} region of the NMSSM

To find the parameter space for our region of interest, $m_{a_1} < 2m_\tau$, we scan the NMSSM parameters using the NMSSMTOOLS package [27–29], applying all known phenomenological and experimental constraints except the following: the cosmological dark matter relic density measured by WMAP [30], the direct $p\bar{p} \to h_1 \to a_1 a_1 \to 4\mu$ search by the Tevatron [31], the direct $e^+e^- \to Zh_1$, $h_1 \to a_1 a_1$ searches by LEP [32,33], the direct $\Upsilon \to \gamma a_1$ searches by CLEO [34] and *BABAR* [35], and limits set by rare $B \to K\ell^+\ell^-$ decays [36]. These important constraints are explicitly studied in our region of interest in a later section.

In our scan, we fix parameters entering the Higgs sector at loop level to $M_1/M_2/M_3 = 150/300/1000$ GeV, $A_t = A_b = A_\tau = 2.5$ TeV, and $M_{f_L} = M_{f_R} = 1$ TeV. We then sample the NMSSM model points uniformly in a six-dimensional space. The first four scan parameters are conventional, broad ranges over the probable values of μ, λ, $\tan\beta$, and A_λ:

(i) $100\ \text{GeV} < \mu < 1000\ \text{GeV}$
(ii) $0 < \lambda < 1$
(iii) $1.5 < \tan\beta < 50$
(iv) $-1\ \text{TeV} < A_\lambda < 5\ \text{TeV}$

For the two remaining parameters, we identify two additional phenomenological variables that allow a more narrow selection of the region of interest and simplify the interpretation of our observations. A theoretical justification of these variables is discussed in the next section. The first of these two parameters, $\mu\kappa/\lambda = \kappa s$, is selected because of its correlation with the mass of the CP-even Higgs bosons; see Fig. 1(a). The corresponding range used in the scan

(v) $0 < \mu\kappa/\lambda < 120\ \text{GeV}$

was chosen to include two equally sized but phenomenologically different subdomains; in the lower one h_1 is light and h_2 is the SM-like Higgs, and in the upper one h_1 is the SM-like Higgs.

The final parameter and its scan range,

(vi) $0\ \text{GeV} < (30\ \text{GeV})\lambda^2 - A_\kappa < 3\ \text{GeV}$,

are chosen to zoom into the region of low a_1 masses as illustrated in Fig. 1(b).

B. Higgs sector spectrum and mixings

The CP-even and CP-odd Higgs mass matrices, $\mathcal{M}_S$ and $\mathcal{M}_P$, can be written as [27]

$$\begin{aligned}
\mathcal{M}^2_{S11} &= g^2 v^2 \sin\beta^2 + \mu \tan\beta(A_\lambda + \kappa s),\\
\mathcal{M}^2_{S22} &= g^2 v^2 \cos\beta^2 + \mu \cot\beta(A_\lambda + \kappa s),\\
\mathcal{M}^2_{S33} &= \lambda A_\lambda \frac{v^2 \sin 2\beta}{2s} + \kappa s(A_\kappa + 4\kappa s),\\
\mathcal{M}^2_{S12} &= (\lambda^2 - g^2/2) v^2 \sin 2\beta - \lambda s(A_\lambda + \kappa s),\\
\mathcal{M}^2_{S13} &= \lambda v(2\lambda s \cos\beta - \sin\beta(A_\lambda + 2\kappa s)),\\
\mathcal{M}^2_{S23} &= \lambda v(2\lambda s \sin\beta - \cos\beta(A_\lambda + 2\kappa s)),
\end{aligned} \tag{3}$$

$$\begin{aligned}
\mathcal{M}^2_{P11} &= \frac{2\lambda s}{\sin 2\beta}(A_\lambda + \kappa s),\\
\mathcal{M}^2_{P22} &= 2\lambda\kappa v^2 \sin 2\beta + \lambda A_\lambda \frac{v^2 \sin 2\beta}{2s} - 3\kappa A_\kappa s,\\
\mathcal{M}^2_{P12} &= \lambda v(A_\lambda - 2\kappa s).
\end{aligned} \tag{4}$$

In general, a_1 is light in the regions of the parameter space approaching either the Peccei-Quinn (PQ) symmetry limit ($\kappa \to 0$) or the R-symmetry (RS) limit ($A_\kappa, A_\lambda \to 0$). In both limits, a_1 is a massless axion, a fact which directly

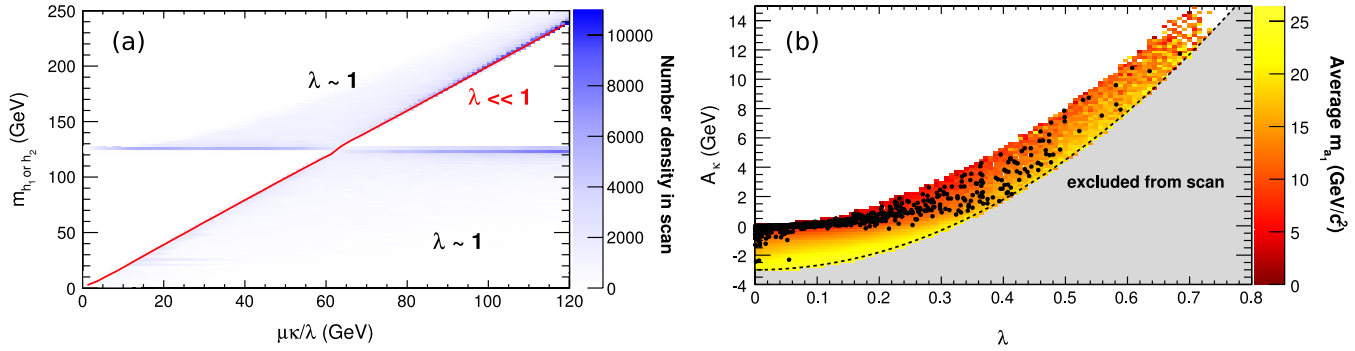

FIG. 1 (color online). (a) Mass of the lightest (h_1) and second-lightest (h_2) CP-even Higgses as a function of $\mu\kappa/\lambda$ and λ. The density of generated scenarios surviving constraints is shown in the blue color scale, and the red line represents the single-valued $\lambda \ll 1$ limit (mean of $\lambda < 0.01$ scenarios). (b) Mass of the lightest CP-odd Higgs (a_1) as a function of A_κ and λ. The color scale is the average mass in each bin, and filled circles are the scenarios with $m_{a_1} < 2m_\tau$. The edge of the low m_{a_1} region follows a parabolic curve, $(30\ \text{GeV})\lambda^2 - A_\kappa \simeq 0$.

follows from Eq. (4). It can be decomposed in terms of the weak eigenstates H_{uI}, H_{dI}, and S_I as (see e.g. [37])

$$a_1 = \cos\theta_P A + \sin\theta_P S_I, \tag{5}$$

where $A = \cos\beta H_{uI} + \sin\beta H_{dI}$. In the PQ limit, the mixing parameters $\cos\theta_P$ and $\sin\theta_P$ are

$$\cos\theta_P = \frac{v\sin 2\beta}{\sqrt{v^2\sin^2 2\beta + 4s^2}}, \qquad \sin\theta_P = -\frac{2s}{\sqrt{v^2\sin^2 2\beta + 4s^2}}. \tag{6}$$

In the RS limit, the same parameters are

$$\cos\theta_P = \frac{v\sin 2\beta}{\sqrt{v^2\sin^2 2\beta + s^2}}, \qquad \sin\theta_P = \frac{s}{\sqrt{v^2\sin^2 2\beta + s^2}}. \tag{7}$$

According to Eqs. (6) and (7), the nonsinglet component of a_1 is determined by the ratio $v\sin 2\beta/s$. Figure 2(a) shows evident correlation of the nonsinglet fraction $1 - \sin^2\theta_P$ of the lightest pseudoscalar Higgs boson a_1 with $v\sin 2\beta/s$, corresponding primarily to the PQ limit, as can be deduced from the slope of the correlation. It also demonstrates that in the region of interest a_1 is nearly a pure singlet, $1 - \sin\theta_P^2 < 1\%$, and that the values of $v\sin 2\beta/s$ are always below 0.1. If we define $\epsilon = v\sin 2\beta/s$, then up to $\mathcal{O}(\epsilon)$, $\mathcal{O}(\kappa^2)$, and $\mathcal{O}(\lambda^2)$, the CP-even Higgs mass matrix can be rewritten as

$$M_S^2 = \lambda s \begin{pmatrix} (A_\lambda + s\kappa)\tan\beta & -(A_\lambda + s\kappa) & \epsilon\left(\frac{\lambda s}{\sin\beta} - \frac{A_\lambda + 2s\kappa}{2\cos\beta}\right) \\ -(A_\lambda + s\kappa) & (A_\lambda + s\kappa)\cot\beta & \epsilon\left(\frac{\lambda s}{\cos\beta} - \frac{A_\lambda + 2s\kappa}{2\sin\beta}\right) \\ \epsilon\left(\frac{\lambda s}{\sin\beta} - \frac{A_\lambda + 2s\kappa}{2\cos\beta}\right) & \epsilon\left(\frac{\lambda s}{\cos\beta} - \frac{A_\lambda + 2s\kappa}{2\sin\beta}\right) & \kappa\frac{A_\kappa + 4s\kappa}{\lambda} \end{pmatrix}. \tag{8}$$

One can see that ϵ also determines the mixing of singlet and nonsinglet CP-even Higgs states. For small values of ϵ and A_κ, characterizing the parameter space relevant to our study, the mass of the singlet CP-even Higgs boson is determined by $2s\kappa = 2\mu\kappa/\lambda$. This substantiates our earlier observation depicted in Fig. 1(a) and the relevance of the $\mu\kappa/\lambda$ parameter used in our scan. Further, in the subdomain $\mu\kappa/\lambda < 60$ GeV, h_1 is light with $m_{h1} \simeq 2\mu\kappa/\lambda$ and has a significant singlet component, particu-

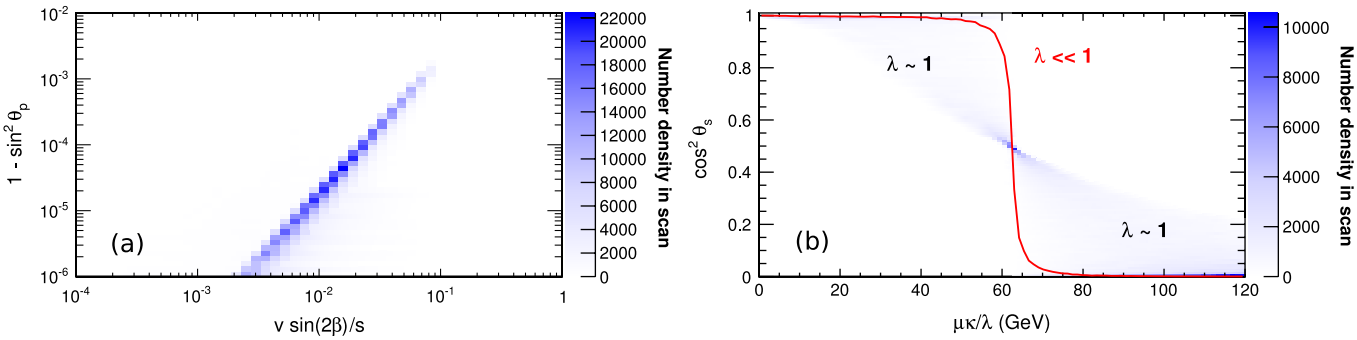

FIG. 2 (color online). (a) Nonsinglet fraction $1 - \sin^2\theta_P$ of the lightest CP-odd Higgs boson (a_1) as a function of $v\sin 2\beta/s$. (b) Singlet fraction $\cos^2\theta_S$ of the lightest CP-even Higgs boson (h_1) as a function of $\mu\kappa/\lambda$. (The red line is the mean of $\lambda < 0.01$ scenarios.)

larly for smaller values of λ (and A_λ). In the upper subdomain $\mu\kappa/\lambda > 60$ GeV, h_1 becomes the SM-like Higgs with $m_{h_1} \simeq 120$ GeV while h_2 acquires a large singlet component and mass $m_{h2} \simeq 2\mu\kappa/\lambda$. This is illustrated in Fig. 2(b) showing the singlet fraction of h_1, the lightest CP-even Higgs boson.

To derive m_{a_1}, we diagonalize the $\mathcal{M}_P$ matrix [Eq. (4)]. Keeping $\mathcal{O}(\kappa)$, $\mathcal{O}(\lambda^2)$, and $\mathcal{O}(\epsilon^2)$ terms, one has

$$m_{a_1}{}^2 = \tfrac{3}{2}(2\mu\kappa/\lambda)^2(\zeta\lambda^2 - A_\kappa), \tag{9}$$

where $\zeta = \frac{3}{2}v^2 \sin 2\beta/\mu$. Because $2\mu\kappa/\lambda$ determines the mass of the predominantly singlet CP-even Higgs boson, $2\mu\kappa/\lambda \geq m_{h_1}$ and is always fairly large. Therefore, a_1 is light if $(\zeta\lambda^2 - A_\kappa)$ is low, motivating the choice of the empirical parameter $(30\ \text{GeV})\lambda^2 - A_\kappa$ used in the scan. The range of this parameter selects a region with m_{a_1} between 0 and approximately 30 GeV, avoiding most of the theoretically inaccessible region in which $\zeta\lambda^2 - A_\kappa < 0$ and therefore $m_{a_1}^2 < 0$, as shown in Fig. 1(b).

C. Higgs couplings and decays

The couplings of h_1 and a_1 to each other and to standard model particles are determined primarily by their singlet and nonsinglet components. While the CP-odd a_1 is always nearly a pure singlet [see Fig. 2(a)], the singlet fraction of h_1 is correlated with $\mu\kappa/\lambda$ but also depends on the smallness of λ. As illustrated by Fig. 2(b), for small λ, h_1 is nearly a pure singlet in the $\mu\kappa/\lambda \lesssim 60$ GeV subregion, while in the $\mu\kappa/\lambda \gtrsim 60$ GeV domain, h_1 has a negligible singlet component and is essentially the SM Higgs. Figure 3 shows a strong suppression of reduced couplings of h_1 to up- and down-type quarks as well as vector bosons in the $\mu\kappa/\lambda \lesssim 60$ GeV domain. This suppression leads to a severe reduction in the production rates of h_1 at colliders, making this scenario challenging for experimental exploration. Fortunately, as will be shown later, small λ values in the low $\mu\kappa/\lambda$ region are excluded by cosmological observations.

Branching fractions of h_1 are determined by relative strength of the h_1 couplings to SM particles and the

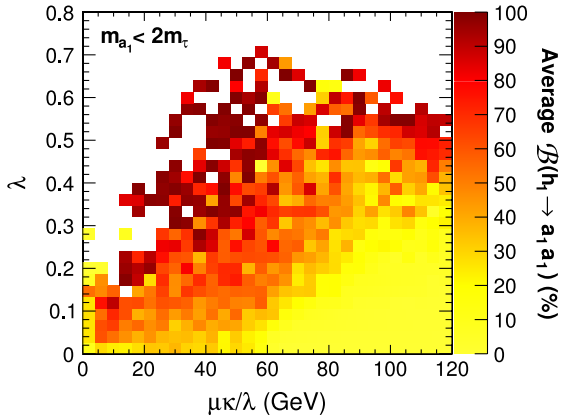

FIG. 4 (color online). Branching fraction of $h_1 \to a_1 a_1$ in the λ versus $\mu\kappa/\lambda$ plane, with the requirement that $m_{a_1} < 2m_\tau$.

$h_1 a_1 a_1$ coupling, which is specific to the NMSSM. Because a_1 has a high singlet fraction, the singlet content of h_1 is directly related to the strength of the $h_1 a_1 a_1$ coupling. If this were the only effect, $\mathcal{B}(h_1 \to a_1 a_1)$ would have been close to 100% in the lower half of the $\mu\kappa/\lambda$ domain and negligible in the upper half. However, this coupling is also proportional to λ [see Eq. (2)], which creates a competing effect as larger values of λ smear the nearly perfect separation of singlet- and doublet-type h_1 in the lower and upper halves of the $\mu\kappa/\lambda$ domain. The overall result is illustrated in Fig. 4, showing average $\mathcal{B}(h_1 \to a_1 a_1)$ for NMSSM models with $m_{a_1} < 2m_\tau$ as a function of $\mu\kappa/\lambda$ and λ. It is evident that the suppression of h_1 SM couplings for $\mu\kappa/\lambda < 60$ GeV makes $\mathcal{B}(h_1 \to a_1 a_1)$ substantial as long as λ is not too small. For the upper part of the $\mu\kappa/\lambda$ domain, $\mathcal{B}(h_1 \to a_1 a_1)$ is small except for large values of λ where the h_1 singlet fraction is enhanced.

As the lightest Higgs boson, a_1 can only decay to SM particles, even though its coupling to SM particles is strongly suppressed due to its nearly singlet nature. One should also notice that a_1 couplings to down-type fermions are proportional to $\tan\beta$ while its couplings to up-type fermions are suppressed as $1/\tan\beta$. Therefore, a_1 branch-

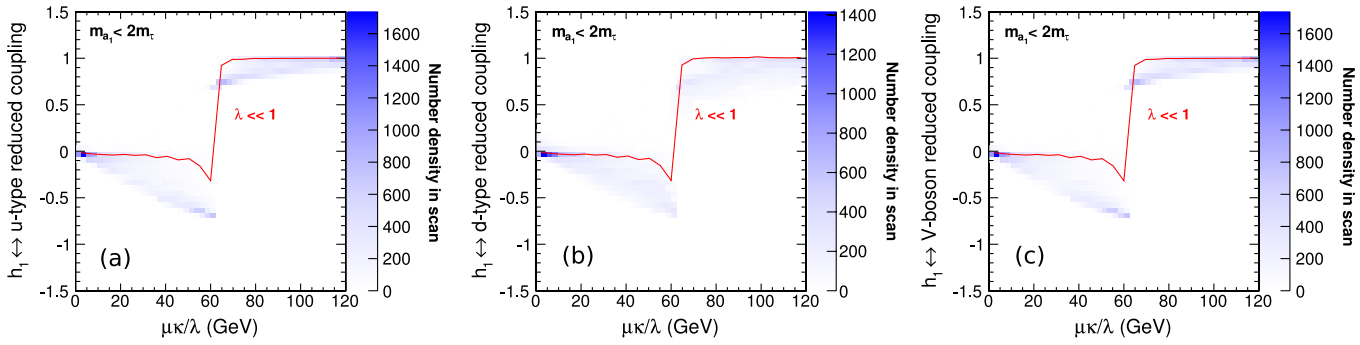

FIG. 3 (color online). Reduced couplings of h_1 to up-type quarks (a), down-type quarks (b), and vector bosons (c) as a function of $\mu\kappa/\lambda$, with the requirement that $m_{a_1} < 2m_\tau$. (The red line is a mean of $\lambda < 0.01$ scenarios.)

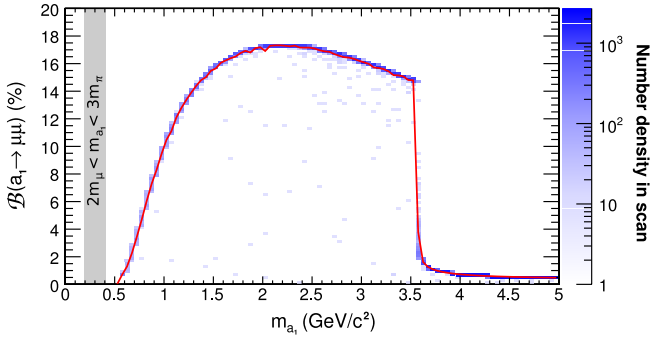

FIG. 5 (color online). Branching fraction of $a_1 \to \mu\mu$ for generated models as a function of m_{a_1}. The red line is a mean of all scenarios as a function of m_{a_1}. The threshold at 3.55 GeV/c^2 is $2m_\tau$. For $2m_\mu < m_{a_1} < 3m_\pi$ (the grey box), the branching fraction would be nearly 100%.

ing fractions follow the standard mass hierarchy of open decay channels to down-type fermions. Figure 5 shows the branching fraction for $a_1 \to \mu\mu$ as obtained using the NMSSMTOOLS package. For $m_{a_1} < 2m_\tau$, the $a_1 \to \mu\mu$ channel becomes significant, making an analysis in the four-muon mode viable for experimental searches.

It is important to note that the NMSSMTOOLS calculation of $\mathcal{B}(a_1 \to \mu\mu)$ shown in Fig. 5 does not include hadronization effects important in the region $m_{a_1} < 1$ GeV/c^2, and therefore is not reliable. One should also notice that for $2m_\mu < m_{a_1} < 3m_\pi$, $\mathcal{B}(a_1 \to \mu\mu)$ is expected to be about 100% because $q\bar{q}$ and gg decays are prohibited by hadronization and spin effects, and because $\gamma\gamma$ is small. Since the status of $\mathcal{B}(a_1 \to \mu\mu)$ in NMSSMTOOLS for $m_{a_1} <$ 0.5 GeV/c^2 is not well established and requires further development, we present our results only for the $m_{a_1} >$ 0.5 GeV region. We would like to notice that $\mathcal{B}(a_1 \to \mu\mu)$ is model dependent in general and can be somewhat different in, for example, the little Higgs model [38] used by the D0 Collaboration in Ref. [31]. Therefore, we present our results as limits on production cross-section times branching ratios for the 4μ signature as a model-independent limit for a given topology and signature under study.

III. CURRENT EXPERIMENTAL CONSTRAINTS

Existing experimental data restrict the NMSSM parameter space for the scenario studied here. In the following, we discuss experimental measurements relevant to this scenario and evaluate their impact in restricting the allowed parameter space for models with low m_{a_1}.

A. Cosmological constraints

The lightest NMSSM neutralino is a candidate for cold dark matter (CDM). The WMAP measurement of the CDM relic density therefore serves as an important constraint on the allowed NMSSM parameter space. In our scan, we used the MICROMEGAS package [39] linked to NMSSMTOOLS to calculate $\Omega_{\rm NMSSM}h^2$ and determine whether a particular model is consistent with the experimental data. We considered a model to be consistent with the CDM measurement if $\Omega_{\rm NMSSM}h^2 \leq 0.1131 + 2 \times 0.0034$, corresponding to the 95% upper limit obtained using the latest WMAP 5-year data set [30]. The NMSSM neutralino relic density need not account for all CDM observed by WMAP, but it cannot exceed it.

To illustrate the effect of the WMAP constraints, Fig. 6(a) shows the density of generated NMSSM models in the λ versus $\mu\kappa/\lambda$ plane under the constraint that $m_{a_1} < 2m_\tau$. Models that were determined to be consistent with the WMAP data are shown in Fig. 6(b). The comparison shows that the WMAP bound excludes the region of small $\mu\kappa/\lambda$ and λ. In that region, the lightest neutralino is light and weakly interacts with SM particles, suppressing the neutralino annihilation rate and enhancing the neutralino relic density to unacceptably large values. Figs. 7(a) and 7(b) make the same comparison but in the m_{a_1} versus m_{h_1} plane.

B. Constraints from direct searches at colliders

Several searches for $h_1 \to a_1 a_1$ have been performed at collider experiments, with the strongest impact on the allowed NMSSM models coming from LEP-II data [33]. Although the singlet component of h_1 at low $\mu\kappa/\lambda$ and λ (and correspondingly low m_{h_1}) would severely suppress h_1 production in $e^+e^- \to h_1 Z$, these extreme scenarios are excluded by the WMAP data. LEP limits [33] on NMSSM models are inferred from $h_1 \to a_1 a_1$, $a_1 \to$ pairs of charm, gluon, and τ jets; $a_1 \to \mu\mu$ limits were not quoted. The LEP-II upper limit on $e^+e^- \to h_1 Z$ with $h_1 \to a_1 a_1$ excludes models that predict m_{h_1} within the kinematic limits, $45 < m_{h_1} < 86$ GeV/c^2, and m_{a_1} in the region of significant detector efficiency, $m_{a_1} > 2$ GeV/c^2.

In addition to LEP data, there were direct searches for $\Upsilon \to \gamma a_1$ by CLEO and *BABAR* at low energy e^+e^- colliders [40,41]. Neither of these searches significantly constrain the NMSSM models with low m_{a_1} because a_1 has a high singlet component, and thus negligible bba_1 coupling [see Fig. 2(a)], for all sampled parameter values. Because CLEO and *BABAR* results have negligible effect on the allowed parameter space, Figs. 6(c) and 7(c) show combined LEP + CLEO + *BABAR* constraints, but the reader is reminded that only LEP constraints are relevant.

The flat $\ell^+\ell^-$ distribution of rare $B \to K\ell^+\ell^-$ decays [42] could potentially set a limit on the parameter space under study through the bound on $\mathcal{B}(B \to Ka_1) \times \mathcal{B}(a_1 \to \mu\mu)$. However, this limit does not actually bound the region of our interest because the coupling of a_1 to up-type and down-type quarks in $b \to sa_1$ penguin diagrams is suppressed due to the highly singlet nature of a_1. For $f_a = \tan\theta_P v \sin(2\beta)/2$, the quantity $f_a \tan^2\beta$ is above 100 TeV in our scan while the charged Higgs mass is typically above 200 GeV/c^2. Thus, the bound set in

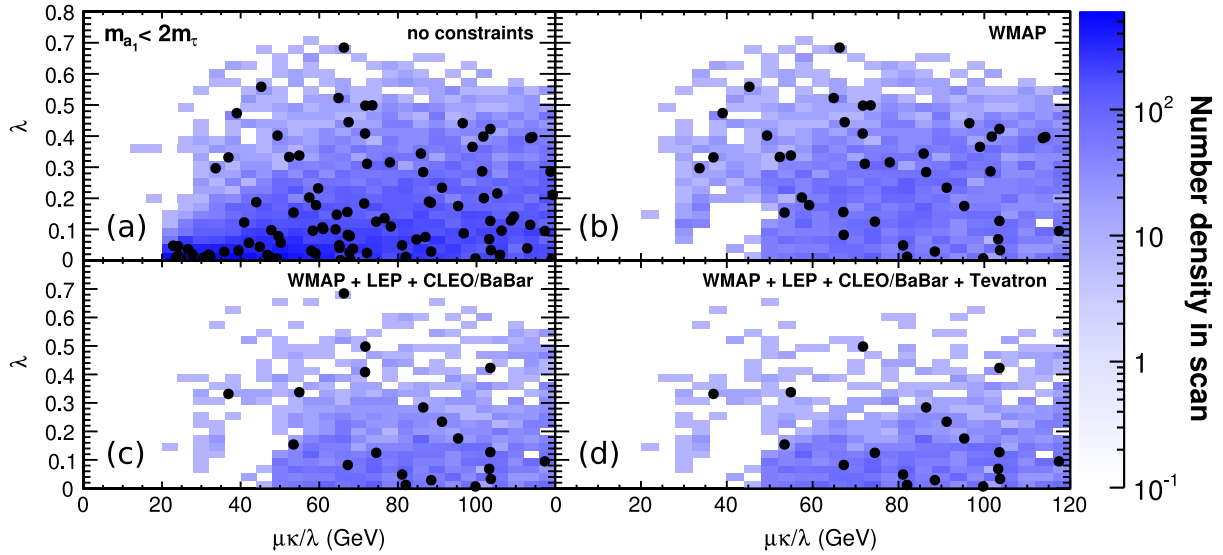

FIG. 6 (color online). Sampled points with $m_a < 2m_\tau$ and experimental constraints successively applied in the λ vs $\mu\kappa/\lambda$ plane. The low energy e^+e^- data (CLEO and *BABAR*) have essentially no impact on the allowed parameter space. Color scale is number density and filled points are 100 models (before application of experimental constraints).

Fig. 2 of Ref. [36] is not relevant to the parameter space of our study.

The results of a search [43] for the NMSSM with a low mass a_1 at the Tevatron was recently published by the D0 Collaboration in the channel $h_1 \to a_1 a_1 \to 4\mu$. With no excess of data over the SM expectations, the paper quotes 95% C.L. upper limits for the cross section of this process. To interpret the D0 result in terms of constraints on allowed NMSSM models in our scan, we calculate the next-to-leading-order (NLO) production cross section for $p\bar{p} \to h_1$ in the NMSSM using the SM NLO calculations for $gg \to H_{\rm SM}$ [44] and $b\bar{b} \to H_{\rm SM}$ with QCD-improved (running) Yukawa couplings [45], corrected for differences in coupling between the SM and the NMSSM using NMSSMTOOLS:

$$\sigma(gg \to h_1) = \sigma(gg \to H_{\rm SM}) \frac{\Gamma(h_1 \to gg)}{\Gamma(H_{\rm SM} \to gg)} = \sigma(gg \to H_{\rm SM}) \frac{{\rm Br}(h_1 \to gg)\Gamma^{\rm tot}(h_1)}{\Gamma(H_{\rm SM} \to gg)}, \quad (10)$$

$$\sigma(b\bar{b} \to h_1) = \sigma(b\bar{b} \to H_{\rm SM}) \left(\frac{Y_{bbh_1}}{Y_{bbH_{\rm SM}}}\right)^2, \quad (11)$$

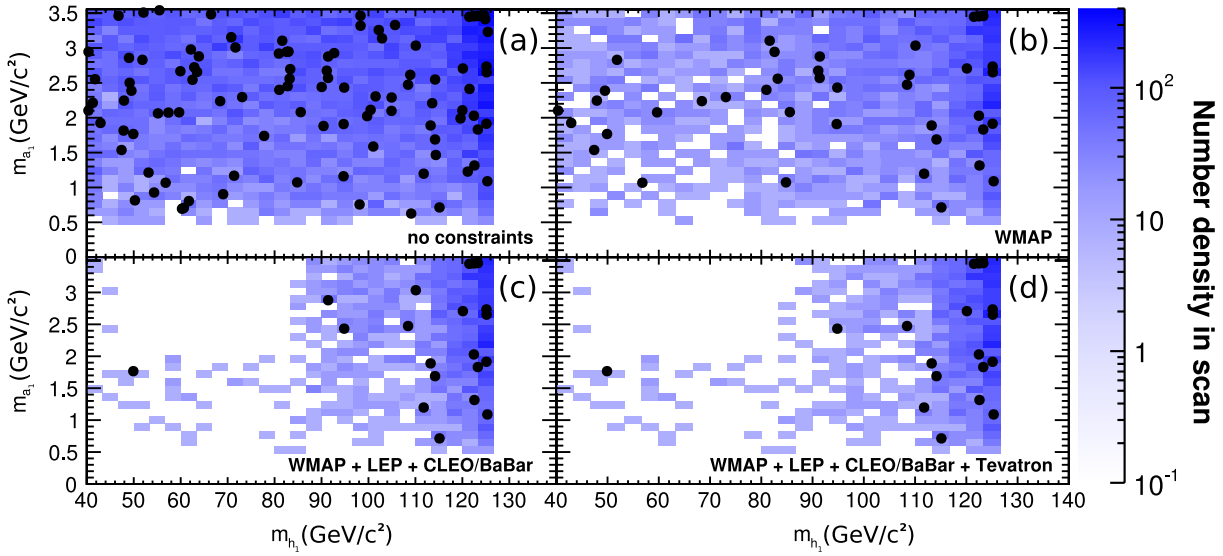

FIG. 7 (color online). Sampled points with $m_a < 2m_\tau$ and experimental constraints successively applied similar to Fig. 6 but in the m_a vs m_h plane. The low energy e^+e^- data (CLEO and *BABAR*) have essentially no impact on the allowed parameter space. Color scale is number density and filled points are 100 models (before application of experimental constraints).

where $\sigma(gg \to H_{\rm SM})$ and $\Gamma(H_{\rm SM} \to gg)$ are calculated using HIGLU [46], while $\mathcal{B}(h_1 \to gg)$, $\Gamma^{\rm tot}(h_1)$, and the ratio of Yukawa couplings $Y_{bbh_1}/Y_{bbH_{\rm SM}}$ are obtained using NMSSMTOOLS. For $\mu\kappa/\lambda < 60$ GeV (non-SM h_1 lighter than 120 GeV/c^2), the cross section is strongly suppressed even compared to the SM for low m_{a_1} because h_1 has a large singlet fraction and weakly couples to SM particles (see Fig. 3). For larger $\mu\kappa/\lambda$, the lightest CP-even Higgs h_1 becomes the SM-like Higgs and has a small $h_1 \to a_1 a_1$ branching fraction.

The D0 paper [43] quotes 95% C.L. limits on $\sigma(p\bar{p} \to h_1) \times B(h_1 \to a_1 a_1 \to 4\mu)$ for several choices of m_{a_1} with $m_{h_1} = 100$ GeV/$c2$. To determine if a particular model in our scan is excluded by these data, we linearly interpolate the published cross-section limits for values of m_{a_1} between the points in [43]. To obtain the experimental cross-section limits as a function of m_{h_1}, we need to correct for variations in the experimental acceptance. We obtain those limits by taking the analysis acceptance to be linear as a function of m_{h_1} "increasing by ~10% when m_{h_1} increases from 80 to 150 GeV/c^2" [43] and matching it to the full analysis acceptance given at $m_{h_1} = 100$ GeV/c^2. We then calculate the production cross-section and branching fractions for the model points and compare them to the values we derive from [43]. Figures 6(d) and 7(d) show the density of NMSSM models surviving WMAP, LEP, and Tevatron constraints. Because of the suppression in production rate at low $\mu\kappa/\lambda$ and small $\mathcal{B}(h_1 \to a_1 a_1)$ at high $\mu\kappa/\lambda$, the Tevatron search has only a limited impact on the allowed NMSSM parameter space, mainly excluding models with high λ. A significant improvement in Tevatron reach for the NMSSM would require a large increase in integrated luminosity, thus requiring the LHC to make a definitive discovery or exclusion of NMSSM models with low m_{a_1}.

IV. A DEDICATED SEARCH FOR THE LOW-m_{a_1} NMSSM AT THE LHC

Since a_1 is only weakly coupled to SM particles, it can be produced only at the LHC via decays of the lightest scalar Higgs $h_1 \to a_1 a_1$. The main characteristic of such a signal at the LHC is two back-to-back (in ϕ) dimuon pairs of spatially nearby muons. The reconstructed dimuon pairs should have invariant masses consistent with one another, and their invariant masses also serve as a direct measurement of m_{a_1}. Additionally, the 4μ invariant mass distribution should have a narrow peak corresponding to the m_{h_1} mass. We use these striking features to design an analysis suitable for early LHC running.

The four-muon final state considered in this analysis has relatively low experimental backgrounds. Therefore, instead of using the vector boson fusion production process chosen in the proposed NMSSM searches targeting the $m_{a_1} > 2m_\tau$ region [25], we focus on the largest Higgs production modes at the LHC, $gg \to h_1$ and $b\bar{b} \to h_1$. We calculate the NLO cross section for $pp \to h_1$ for the NMSSM by rescaling the LHC SM NLO calculations [44,45] to correct for differences in couplings between the SM and NMSSM [Eqs. (10) and (11)]. Like the Tevatron case, the cross section is strongly suppressed compared to the SM if h_1 has a large singlet fraction. Figure 8 shows the production cross section for 14 TeV $pp \to h_1 + X$ as a function of $\mu\kappa/\lambda$. While this suppression makes the analysis challenging even at the LHC, the constraints arising from the WMAP relic density measurement exclude models with very low values of λ, so the allowed models have small but non-negligible production cross sections.

A. Analysis selections

We use PYTHIA to generate signal event templates with m_{h_1} in the range from 70 to 140 GeV/c^2 and m_{a_1} in the range from 0.5 to 4 GeV/c^2. We chose the CMS detector as a benchmark for modeling a realistic experimental environment, with parameters described in Ref. [47]. The important parameters for this analysis are muon momentum resolution, the minimum muon momentum needed to reach the muon system, geometric acceptance, and the average muon reconstruction efficiencies. Because of the large number of reconstructed muons in the event, we take the trigger efficiency to be 100%.

The analysis starts by requiring at least four muon candidates with transverse momentum $p_T > 5$ GeV/c and pseudorapidity $|\eta| < 2.4$ to ensure high and reliable reconstruction efficiency. Of the four muon candidates, at least one must have $p_T > 20$ GeV/c to suppress major backgrounds and to satisfy trigger requirements. Each event is required to have at least two positively charged and two negatively charged muon candidates. For the surviving events, we define quadruplets of candidates, pairing the candidates by charge and sorting them into two dimuon pairs by minimizing the quantity $(\Delta R(\mu_i, \mu_j)^2 + \Delta R(\mu_k, \mu_l)^2)$, where $\Delta R^2 = \Delta\eta^2 + \Delta\phi^2$. Muon quadruplets for which $\Delta R > 0.5$ in either of the pairs are discarded as inconsistent with the signal topology. Acceptance for the selections listed above is shown in Fig. 9 for several representative values of m_{h_1} and m_{a_1}.

The requirement of four sufficiently energetic muons in the event dramatically reduces contributions of potential backgrounds for this analysis. After acceptance selections, the dominant background is due to the QCD multijet production where muons originate from heavy-flavor resonances, from heavy-flavor quark decays, or from π/K decays in flight. We use PYTHIA to estimate the QCD multijet background and obtain approximately 2.6 events/pb^{-1} (approximately half containing at least one decay in flight). Using CALCHEP [48] to estimate $pp \to 4\ell + X$ electroweak backgrounds, we obtain

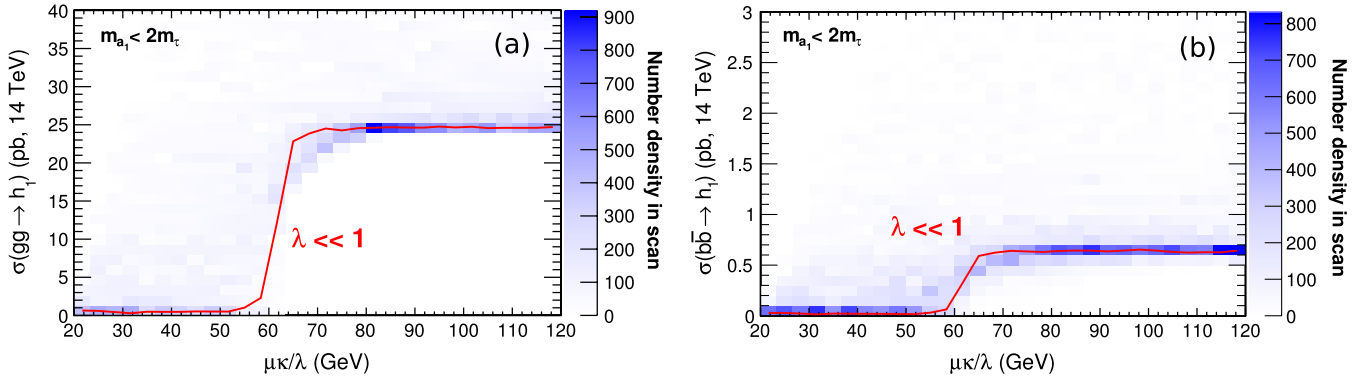

FIG. 8 (color online). Contributions to the $pp \to h_1$ production cross section at $\sqrt{s} = 14$ TeV as a function of $\mu\kappa/\lambda$ and λ, from gg (a) and $b\bar{b}$ (b), with the requirement that $m_{a_1} < 2m_\tau$. (The red line is a mean of $\lambda < 0.01$ scenarios.)

0.04 events/pb^{-1}. Direct J/ψ production is found by PYTHIA to be completely negligible. Other SM backgrounds (top, W + jets) are negligible in the region of interest of this analysis.

The backgrounds are further reduced by requiring the kinematics to be consistent with the expected signal signature. We calculate the invariant mass of each of dimuon pair, m_{12} and m_{34}, as well as the invariant mass of all four muons, denoted as m_{1234}. Figure 10(a) shows the invariant mass of the muon pairs passing all selections in signal events for two choices of m_{h_1} and m_{a_1}. Figure 10(b) shows the distribution of m_{1234} for two benchmark points. To focus on the region of interest, we require $m_{1234} > 60$ GeV/c^2, m_{12}, $m_{34} < 4$ GeV/c^2, which reduces the QCD background to 0.4 events/pb^{-1}.

To ensure the compatibility of the measured invariant masses of the two dimuon pairs, one could require $|m_{12} - m_{34}| < 0.08 + 0.005 \times (m_{12} + m_{34})$. Such cut would require the two pair masses to be consistent with each other and would take into account the widening of absolute resolution in the reconstructed dimuon mass as a function of mass. If applied, the only background that still may be not completely negligible is the QCD multijet production, for which we conservatively estimate the upper bound to be 0.02 events/pb^{-1}. However, instead of applying this selection explicitly, a better approach would be to fit the data in the 3D space (m_{12}, m_{34}, m_{1234}), taking into account kinematic properties of the signal events. This approach maximizes the signal acceptance and therefore the statistical power of the analysis. It is also convenient from an experimental standpoint as the background events are distributed smoothly over the 3D space, allowing a fit of the 3D distribution to estimate backgrounds directly from the data. A potential signal would appear as a concentration of events in a small region of the space (a 3D peak). We use a binned likelihood defined as a function of parameters m_{a_1}, m_{h_1}, and effective signal cross-section $\sigma \times \mathcal{B}(h_1 \to a_1 a_1)\mathcal{B}^2(a_1 \to \mu\mu)$ to fit the simulated data using either background-only or signal-plus-background templates. We estimate the sensitivity of this analysis and present it in terms of the 95% C.L. exclusion levels for signal cross section using a Bayesian technique.

Our estimations show that for an early data search ($\mathcal{L} \simeq 100$ pb^{-1}), the backgrounds are negligible (see Table I).

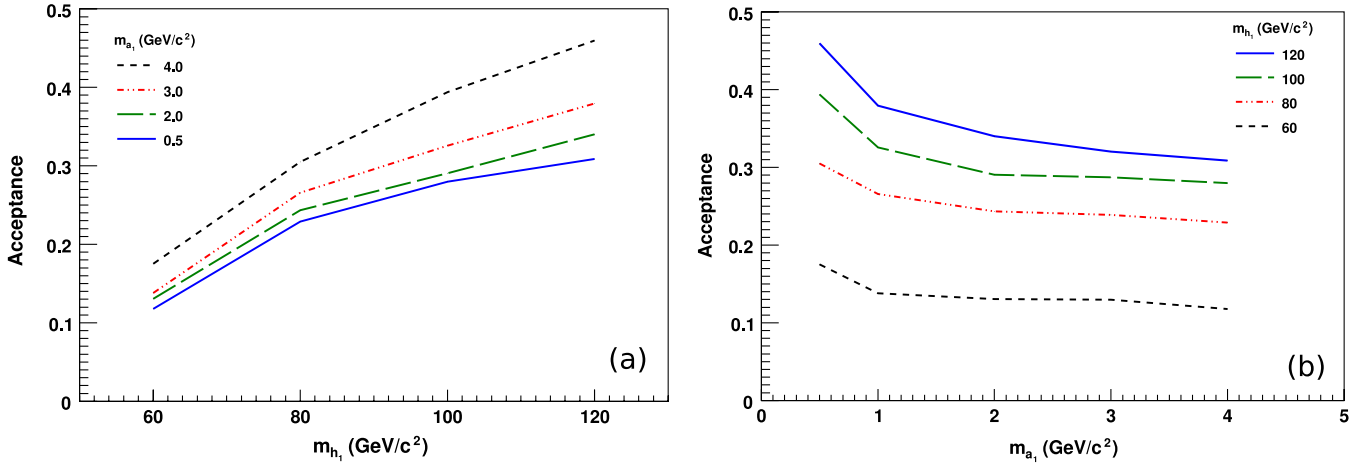

FIG. 9 (color online). (a) Acceptance as a function of m_{a_1} for fixed m_{h_1}. (b) Acceptance as a function of m_{h_1} for fixed m_{a_1}.

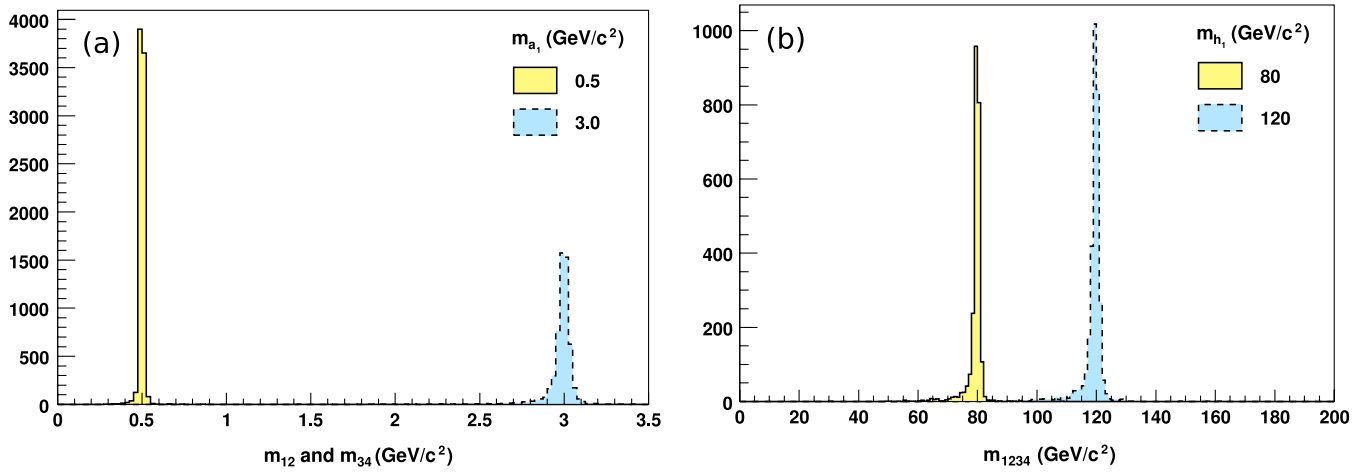

FIG. 10 (color online). (a) Invariant mass of reconstructed muon pairs for $m_{a_1} = 0.5$ and 3 GeV/c^2 (in both cases $m_{h_1} = 100$ GeV/c^2). (b) Invariant mass of four reconstructed muons for $m_{h_1} = 80$ and 120 GeV/c^2 (in both cases $m_{a_1} = 3.0$ GeV/c^2).

For an analysis with higher luminosity, one can restore the zero-background situation by adding an isolation requirement to one or both of the dimuon pairs in the event. Isolation can be defined either by setting an upper bound on the sum of the transverse momenta of all tracks in a cone around the reconstructed direction of the dimuon pair, excluding two muon tracks, or by rejecting pairs with additional tracks above a certain threshold. For the analysis with $\mathcal{L} = 1$ fb^{-1} of data, we required no charged tracks with momentum $p_T > 1$ GeV/c in the $\sqrt{(\Delta\eta)^2 + (\Delta\phi)^2} < 0.3$ cone around the direction of at least one of the two muon pairs. This requirement is 96% efficient for signal and reduces QCD multijet background, dominated by events with muons originating from heavy-flavor jets, by a factor of 6–7. For high-luminosity data sets, isolation can be further tightened to increase background suppression with only a moderate loss in signal efficiency.

B. LHC reach for NMSSM $h_1 \to a_1 a_1$

We have proposed an analysis that has a potential of discovering the NMSSM with early LHC data in scenarios with low m_{a_1}. We estimate its sensitivity by calculating the 95% C.L. upper limit on the product $\sigma(pp \to h)\mathcal{B}(h_1 \to a_1 a_1)\mathcal{B}^2(a_1 \to \mu\mu)\alpha$, where α is the analysis acceptance, using a Bayesian technique. Because of the low background, an upper limit on the signal corresponds to approximately three reconstructed events. This limit is 0.0293 pb for $\mathcal{L} = 100$ pb^{-1} and scales linearly with luminosity, assuming that the number of observed background events is zero. In nearly all pseudoexperiments, this limit is independent of m_{h_1} and m_{a_1} because the effective signal region that dominates signal significance is essentially background-free and the probability to observe an event is small. Note that the corresponding projection for $\mathcal{L} = 1$ fb^{-1} includes the isolation cut, slightly reducing signal efficiency and correspondingly loosening the limit. The upper limit on $\sigma(pp \to h_1)\mathcal{B}(h_1 \to a_1 a_1)$ is shown as a function of m_{h_1} and m_{a_1} in Table II.

Figure 11 presents the region of NMSSM parameter space excluded by the Tevatron and the region that the LHC would exclude with 100 pb^{-1} (without isolation) and 1 fb^{-1} (with isolation), assuming no observed signal. The regions are presented in the λ, $\mu\kappa/\lambda$ plane [Fig. 11(a)], the m_{a_1}, m_{h_1} plane [Fig. 11(b)], and the plane of $h_1 \to a_1 a_1 \to 4\mu$ branching fraction versus LHC $pp \to h_1$ cross section [Fig. 11(c)]. High h_1-singlet scenarios (which have low production cross sections) and low h_1-singlet scenarios (which have low $h_1 \to a_1 a_1$ branching fractions) are accessible to the Tevatron and the LHC to different degrees, leading to a region in Fig. 11(c) where high h_1-singlet scenarios are excluded by the Tevatron while some low h_1-singlet models with the same LHC cross-section times branching fraction are not. The Tevatron exclusion region has a sharp border only when viewed as a function of the Tevatron cross section.

It is worth noting that quantitative background estimates performed in our analysis may indicate that the LHC reach for NMSSM models with $m_{a_1} > 2m_\tau$ in the $2\mu 2\tau$ channel are substantially weaker than suggested in Ref. [26], which relied on extrapolating QCD backgrounds to avoid high-statistics simulations. Though the 4μ and $2\mu 2\tau$ analyses apply different selections, a rough extrapolation of the simulated QCD multijet backgrounds to the 4μ channel yields an estimate of backgrounds to the $2\mu 2\tau$ channel that is 3 orders of magnitude larger than what was used in Ref. [26], even without considering the much larger misidentification rate of hadronically decaying taus. The expected number of QCD multijet events in the $m_{1234} > 60$, m_{12} and $m_{34} < 4$ GeV/c^2 region of the 4μ analysis, which is 390 ± 90 events/fb^{-1} (note that the numbers in Table I are for 100 pb^{-1}), could be reduced by a factor of 10–20 using tight isolation requirements. Unlike our analysis, the study in Ref. [26] applies restrictions on the transverse

TABLE I. Expected rate of background events per 100 pb^{-1} of luminosity after selection.

Selection	4 leptons	QCD multijet
$p_T(\mu_1) > 20$ GeV/c and $p_T(\mu_i) > 5$ GeV/c; $i = 2, 3, 4$	4.8 ± 0.2	267 ± 23
$m_{12}, m_{34} < 4$ GeV/c^2	0.024 ± 0.012	90 ± 13
$m_{1234} > 60$ GeV/c^2	0.010 ± 0.007	39 ± 9
$\lvert m_{12} - m_{34}\rvert < 0.08$ GeV/$c^2 + 0.005 \times (m_{12} + m_{34})$	$0.000^{+0.005}_{-0.000}$	$0.00^{+1.95}_{-0.00}$

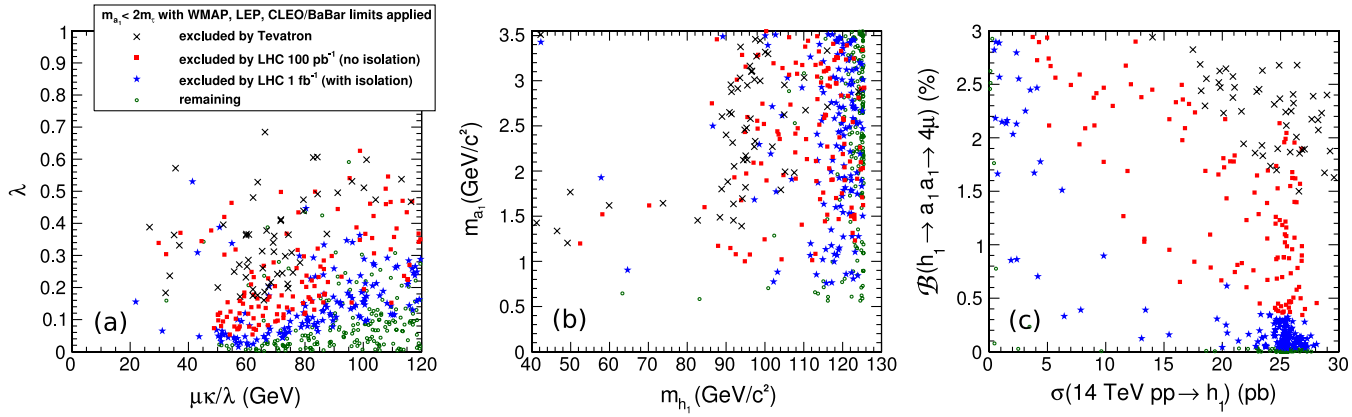

FIG. 11 (color online). Sampled models with $m_{a_1} < 2m_\tau$ and all experimental constraints applied, presented as a function of model parameters (a), Higgs masses (b), branching fraction and LHC cross section (c). With only 100 pb^{-1}, the LHC's reach extends beyond that of the Tevatron.

momentum of the dimuon pair, $p_T^{\mu\mu} > 40$ GeV/c, and on the missing transverse energy $\not{E}_{\rm T} > 30$ GeV. However, the $p_T^{\mu\mu}$ selection is similar to $m_{1234} > 60$ GeV/c^2 and, given typical expected $\not{E}_{\rm T}$ resolution for multijet events, a $\not{E}_{\rm T} > 30$ GeV requirement cannot be powerful enough to overcome several orders of magnitude in estimated event count. Scaling the 4μ background estimate down by a factor of 10 to account for muon isolation, we expect about 39 ± 9 events/fb^{-1} from QCD multijets, as opposed to the 0.03 events/fb^{-1} in Ref. [26]. Allowing for the larger rate of tau misidentification compared to muons only increases the discrepancy. Another argument can be made using the D0 measurement in the $2\mu 2\tau$ channel [43], which had 1–2 expected background events in the narrow ($\pm$ 0.3–1.0 GeV/c^2) windows around the selected points in the dimuon mass. Using common scaling estimates of background contributions from the Tevatron to the LHC, one would expect similar backgrounds for LHC data sets of the order of 100 pb^{-1}. For data sets with integrated luminosities of the order of 500 pb^{-1}, the corresponding QCD contamination would be 5–10 events per window. These much larger background estimates severely affect achievable exclusion limits and, considering trial factors, would make any discovery in the $2\mu 2\tau$ channel with early data extremely challenging.

TABLE II. The 95% C.L. upper limit on $\sigma(pp \to h_1) \times \mathcal{B}(h_1 \to a_1 a_1 \to 4\mu)$ (fb) at the LHC with $\mathcal{L} = 100$ pb^{-1} (no isolation) and $\mathcal{L} = 1$ fb^{-1} (with isolation). The limit tightens at high m_{h_1} because of the increase in acceptance with m_{h_1}.

	m_{a_1} (GeV/c^2)				
	0.5	1.0	2.0	3.0	4.0
$\mathcal{B}(a_1 \to \mu\mu)$ (%)	0[a]	9.8	15.2	16.2	0.7
for $\mathcal{L} = 100$ pb^{-1} (no isolation)					
$m_{h_1} = 80$ GeV/c^2	96.0	110.3	121.1	122.6	126.1
$m_{h_1} = 100$ GeV/c^2	74.8	90.3	100.8	102.4	103.9
$m_{h_1} = 120$ GeV/c^2	63.9	77.4	86.0	90.8	94.4
for $\mathcal{L} = 1000$ pb^{-1} (with isolation)					
$m_{h_1} = 80$ GeV/c^2	10.0	11.5	12.6	12.8	13.1
$m_{h_1} = 100$ GeV/c^2	7.8	9.4	10.5	10.7	10.8
$m_{h_1} = 120$ GeV/c^2	6.7	8.1	9.0	9.5	9.8

[a]Recall that $\mathcal{B}(h_1 \to a_1 a_1)$ is obtained using NMSSMTOOLS and is not reliable for $m_{a_1} \lesssim 1$ GeV/c^2. Furthermore, this branching fraction is expected to reach nearly 100% for $2m_\mu < m_{a_1} < 3m_\tau$.

V. CONCLUSIONS

We have studied the phenomenology of the NMSSM scenarios with the mass of the lowest CP-odd Higgs boson, a_1, below the 2τ threshold. Our analysis of the impact of existing data on these models has shown that the WMAP

and LEP-II data provide the most constraining power, while recent CLEO and *BABAR* measurements have essentially no impact on the allowed parameter space, and the Tevatron data have only a weak impact on the allowed parameter space. As a result, a large fraction of the parameter space is not excluded by any existing data. We conclude that a new analysis should be performed at the LHC to definitively confirm or exclude these models. We propose an analysis suitable for the LHC using the 4μ signature, which has very low backgrounds and striking kinematical features allowing direct and precise measurement of the masses of the a_1 and h_1 bosons. Using the CMS experiment as a benchmark, we estimate the sensitivity of such an analysis and demonstrate that it has the potential to either make a discovery or significantly diminish the allowed parameter space of the NMSSM with low m_{a_1} using only 100–1000 pb^{-1} of early LHC data.

ACKNOWLEDGMENTS

We thank Ulrich Ellwanger, Cyril Hugonie, Alexander Pukhov, and Jay Wacker for useful discussions. One of the authors (A. B.) would like to thank the GGI Institute (Florence), and another (J. P.) would like to thank Fermilab, where important parts of the work on the paper were performed. This work would not be possible without the support of the U.S. Department of Energy, the State of Texas, and the Universities Research Association Visiting Scholars Program.

[1] H. P. Nilles, M. Srednicki, and D. Wyler, Phys. Lett. **120B**, 346 (1983).
[2] J. M. Frere, D. R. T. Jones, and S. Raby, Nucl. Phys. **B222**, 11 (1983).
[3] J. R. Ellis, J. F. Gunion, H. E. Haber, L. Roszkowski, and F. Zwirner, Phys. Rev. D **39**, 844 (1989).
[4] M. Drees, Int. J. Mod. Phys. A **4**, 3635 (1989).
[5] U. Ellwanger, Phys. Lett. B **303**, 271 (1993).
[6] U. Ellwanger, M. Rausch de Traubenberg, and C. A. Savoy, Phys. Lett. B **315**, 331 (1993).
[7] T. Elliott, S. F. King, and P. L. White, Phys. Rev. D **49**, 2435 (1994).
[8] P. N. Pandita, Z. Phys. C **59**, 575 (1993).
[9] U. Ellwanger, M. Rausch de Traubenberg, and C. A. Savoy, Z. Phys. C **67**, 665 (1995).
[10] S. F. King and P. L. White, Phys. Rev. D **52**, 4183 (1995).
[11] F. Franke and H. Fraas, Int. J. Mod. Phys. A **12**, 479 (1997).
[12] U. Ellwanger, M. Rausch de Traubenberg, and C. A. Savoy, Nucl. Phys. **B492**, 21 (1997).
[13] D. J. Miller, R. Nevzorov, and P. M. Zerwas, Nucl. Phys. **B681**, 3 (2004).
[14] J. E. Kim and H. P. Nilles, Phys. Lett. **138B**, 150 (1984).
[15] R. Dermisek and J. F. Gunion, Phys. Rev. Lett. **95**, 041801 (2005).
[16] A. Menon, D. E. Morrissey, and C. E. M. Wagner, Phys. Rev. D **70**, 035005 (2004); D. G. Cerdeno, C. Hugonie, D. E. Lopez-Fogliani, C. Munoz, and A. M. Teixeira, J. High Energy Phys. 12 (2004) 048; G. Belanger, F. Boudjema, C. Hugonie, A. Pukhov, and A. Semenov, J. Cosmol. Astropart. Phys. 09 (2005) 001; J. F. Gunion, D. Hooper, and B. McElrath, Phys. Rev. D **73**, 015011 (2006); F. Ferrer, L. M. Krauss, and S. Profumo, Phys. Rev. D **74**, 115007 (2006); D. G. Cerdeno, E. Gabrielli, D. E. Lopez-Fogliani, C. Munoz, and A. M. Teixeira, J. Cosmol. Astropart. Phys. 06 (2007) 008; C. Hugonie, G. Belanger, and A. Pukhov, J. Cosmol. Astropart. Phys. 11 (2007) 009; V. Barger, P. Langacker, I. Lewis, M. McCaskey, G. Shaughnessy, and B. Yencho, Phys. Rev. D **75**, 115002 (2007); S. Kraml, A. R. Raklev, and M. J. White, Phys. Lett. B **672**, 361 (2009); G. Belanger, C. Hugonie, and A. Pukhov, J. Cosmol. Astropart. Phys. 01 (2009) 023.
[17] B. A. Dobrescu, G. L. Landsberg, and K. T. Matchev, Phys. Rev. D **63**, 075003 (2001); B. A. Dobrescu and K. T. Matchev, J. High Energy Phys. 09 (2000) 031.
[18] J. F. Gunion, H. E. Haber, and T. Moroi, arXiv:hep-ph/9610337; U. Ellwanger, J. F. Gunion, and C. Hugonie, arXiv:hep-ph/0111179.
[19] J. R. Ellis, J. F. Gunion, H. E. Haber, L. Roszkowski, and F. Zwirner, Phys. Rev. D **39**, 844 (1989); B. A. Dobrescu, G. L. Landsberg, and K. T. Matchev, Phys. Rev. D **63**, 075003 (2001); U. Ellwanger, J. F. Gunion, C. Hugonie, and S. Moretti, arXiv:hep-ph/0305109; arXiv:hep-ph/0401228; U. Ellwanger, J. F. Gunion, and C. Hugonie, J. High Energy Phys. 07 (2005) 041.
[20] S. Moretti, S. Munir, and P. Poulose, Phys. Lett. B **644**, 241 (2007).
[21] S. Chang, P. J. Fox, and N. Weiner, Phys. Rev. Lett. **98**, 111802 (2007).
[22] R. Dermisek and J. F. Gunion, Phys. Rev. D **75**, 075019 (2007).
[23] K. Cheung, J. Song, and Q. S. Yan, Phys. Rev. Lett. **99**, 031801 (2007).
[24] J. R. Forshaw, J. F. Gunion, L. Hodgkinson, A. Papaefstathiou, and A. D. Pilkington, J. High Energy Phys. 04 (2008) 090.
[25] A. Belyaev, S. Hesselbach, S. Lehti, S. Moretti, A. Nikitenko, and C. H. Shepherd-Themistocleous, arXiv:0805.3505.
[26] M. Lisanti and J. G. Wacker, Phys. Rev. D **79**, 115006 (2009).
[27] U. Ellwanger, J. F. Gunion, and C. Hugoine, J. High Energy Phys. 02 (2005) 066.
[28] U. Ellwanger and C. Hugoine, Comput. Phys. Commun. **175**, 290 (2006).

[29] F. Domingo and U. Ellwanger, J. High Energy Phys. 12 (2007) 090.
[30] D. N. Spergel *et al.* (WMAP Collaboration), Astrophys. J. Suppl. Ser. **148**, 175 (2003); C. L. Bennett *et al.* (WMAP Collaboration), Astrophys. J. Suppl. Ser. **148**, 1 (2003); D. N. Spergel *et al.* (WMAP Collaboration), Astrophys. J. Suppl. Ser. **170**, 377 (2007); E. Komatsu *et al.* (WMAP Collaboration), arXiv:astro-ph/0803.0547.
[31] V. M. Abazov *et al.* (D0 Collaboration), Phys. Rev. Lett. **103**, 061801 (2009).
[32] G. Abbiendi *et al.* (OPAL Collaboration), Eur. Phys. J. C **18**, 425 (2001).
[33] G. Abbiendi *et al.* (OPAL Collaboration), Eur. Phys. J. C **27**, 483 (2003).
[34] W. Love *et al.* (CLEO Collaboration), Phys. Rev. Lett. **101**, 151802 (2008).
[35] B. Aubert *et al.* (*BABAR* Collaboration), Phys. Rev. Lett. **103**, 081803 (2009).
[36] M. Freytsis, Z. Ligeti, and J. Thaler, Phys. Rev. D **81**, 034001 (2010).
[37] U. Ellwanger, C. Hugonie, and A. M. Teixeira, arXiv:0910.1785.
[38] K. Cheung, J. Song, P. Tseng, and Q.-S. Yan, Phys. Rev. D **78**, 055015 (2008).
[39] G. Belanger, F. Boudjema, C. Hugonie, A. Pukhov, and A. Semenov, J. Cosmol. Astropart. Phys. 09 (2005) 001.
[40] D. Besson *et al.* (CLEO Collaboration), Phys. Rev. D **76**, 072008 (2007).
[41] B. Aubert *et al.* (*BABAR* Collaboration), Phys. Rev. Lett. **103**, 081803 (2009).
[42] I. Adachi *et al.* (Belle Collaboration), arXiv:0810.0335.
[43] V. M. Abazov *et al.* (D0 Collaboration), Phys. Rev. Lett. **103**, 061801 (2009).
[44] M. Spira, A. Djouadi, D. Graudenz, and P. M. Zerwas, Nucl. Phys. **B453**, 17 (1995).
[45] C. Balazs, H. J. He, and C. P. Yuan, Phys. Rev. D **60**, 114001 (1999).
[46] M. Spira, Nucl. Instrum. Methods Phys. Res., Sect. A **389**, 357 (1997).
[47] CMS Collaboration, CERN Reports No. CERN-LHCC-2006-001 and No. CERN-LHCC-2006-028, 2006.
[48] A. Pukhov, arXiv:hep-ph/0412191.